

DEVELOPMENTS IN MODELLING OF GAS INJECTION AND SLAG FOAMING

Gordon A. IRONS

McMaster University, Hamilton, Ontario, L8S 4L7, CANADA

ABSTRACT

Gas injection into metallurgical ladles has been an active area of CFD modelling for many years. Recent work with both Eulerian and Lagrangian frameworks is presented for bottom stirring in ladle and steelmaking electric furnace configurations. Comparison with water and liquid metal results shows that the Lagrangian models provide a better representation of the systems. Slag foaming is an important phenomenon in smelting-reduction processes and electric furnace steelmaking. The void fraction in the foam is generally greater than 0.9, a regime that has received considerably less attention than bottom stirring where the local void fraction is less than 0.1. Again, it was found, by comparison with experimental data, that Lagrangian models were generally preferable over Eulerian models.

NOMENCLATURE

C_D :	drag coefficient
C_L :	lifting coefficient
C_{VM} :	virtual mass coefficient of bubbles
F:	force
M_L :	interfacial momentum exchange for liquid phase
P:	dynamic pressure or turbulent energy caused by shear work of bubbles
S:	source terms
T:	time of bubble tracking
U:	velocity in θ direction
V:	velocity in r direction or volume
W:	velocity in z direction
\vec{g} :	gravitational acceleration
$\vec{i}, \vec{j}, \vec{k}$:	unit vectors in r, θ , z directions
\vec{S}_V :	source term for velocity components
d:	equivalent bubble diameter
k:	turbulent kinetic energy or reaction rate constant
r:	radius direction co-ordinate
s:	distance in the θ direction
t:	time
z:	vertical direction co-ordinate
Φ :	general variable
Γ :	general diffusion coefficient
α :	volume fraction
μ :	viscosity
μ_{eff} :	effective viscosity
μ_t :	turbulent viscosity

θ :	angular direction co-ordinate
ρ :	density
$>$:	random number of Gaussian distribution

Subscripts

b, bub:	bubble
f:	fluctuation
g:	gas phase
l:	liquid phase
t:	turbulence or total
B:	buoyancy
D:	drag
EP:	Turbulent kinetic energy dissipation rate
L:	lift
M:	mass
R:	relative (velocity)

INTRODUCTION

There are two basic formulation schemes used for the simulations of gas-liquid flows: the Eulerian-Lagrangian formulation, and the Eulerian-Eulerian formulation. For the sake of brevity, these schemes will simply be referred to as Lagrangian and Eulerian schemes, respectively. In the Lagrangian formulation, the liquid phase equations are solved in a fixed or Eulerian frame of reference, similar to a single-phase calculation, and the bubble phase equations are solved with the bubbles as the Lagrangian frame of reference. Velocities and void fraction distribution of the phase are obtained by tracking a large number of bubbles and averaging, so that the gas void fraction is defined without ambiguity. Because the phases are computed with different schemes it is vitally important that quantities transported across the interface are conserved in conformity with the jump conditions; this aspect has not been carefully addressed in the metallurgical literature. The Eulerian formulation does not require this conversion. However, in ladles the gas phase is an unconfined plume with a free boundary between it and the liquid-only region. It is therefore vital to prevent the gas phase from numerically diffusing into regions where no bubbles are present in reality. This is a challenging task for the Eulerian formulation because the liquid phase flows in a circulating mode and numerical diffusion is an inherent weakness of these methods. These aspects have not been discussed in detail in papers published in the metallurgical literature.

GAS INJECTION

Introduction

For over 20 years the injection of gases into ladles containing liquid steel has been an active area of research and industrial interest. Much of this work has been reviewed recently by Mazumdar and Guthrie. More recently, Sheng and Irons (1995) have developed Lagrangian models for gas-stirred ladles. To utilize these models requires good knowledge of the bubble drag coefficients in the plume; several relationships have been proposed, but none extensively tested against experimental data. By means of a combined electrical probe-laser doppler anemometry system Sheng and Irons (1992) were able to measure liquid velocity, bubble velocity and void fraction for a wide range of bubble sizes inside plumes. The results are shown in Figure 1. Quite surprisingly, the drag coefficients were very close to those expected for single bubbles of the same size, and were independent of the void fraction. Some modellers have assumed this to be true, others have used correlations which have a void fraction dependence.

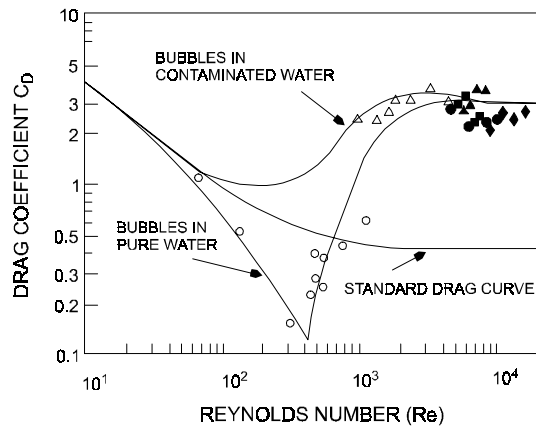


Figure 1: Drag coefficients for single bubbles in pure and contaminated water compared with data for bubbles rising in unconfined plumes in water. The standard drag coefficient for spheres is also shown.

Another major issue in the plume dynamics is the spread of the plume as it rises. Early models required the *a priori* imposition of this feature. Sheng and Irons (1995) have shown that the bubble dispersion can be accounted for by the lateral lift force. The concept, shown schematically in Figure 2, shows that a bubble will move laterally down a radial gradient of vertical velocity, akin to the curve of a spinning baseball. With the detailed measurements, the lateral lift coefficient was extracted from the data; as Figure 3 shows, the coefficients fall within the range of previous work with much smaller bubbles. An additional factor considered in that work was bubble break-up. By not accounting for this phenomenon the void fraction is considerably over-estimated as shown in Figure 4. Therefore, with the validated drag coefficients and lateral lift coefficients, and information on bubble

break-up, more accurate descriptions of the plume dynamics were established.

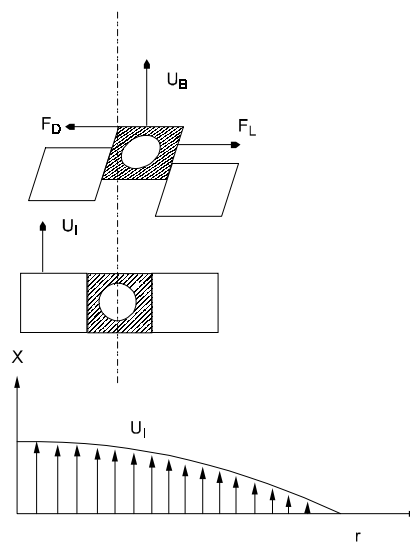


Figure 2: The concept of lateral lift, showing that a bubble will move “down” a velocity gradient.

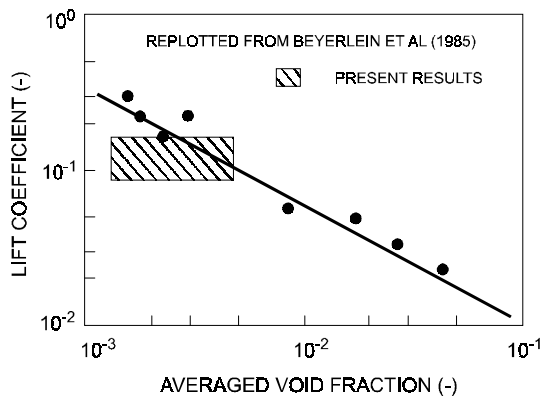


Figure 3: Lateral lift coefficients measured in plumes (present results) compared with smaller single bubbles.

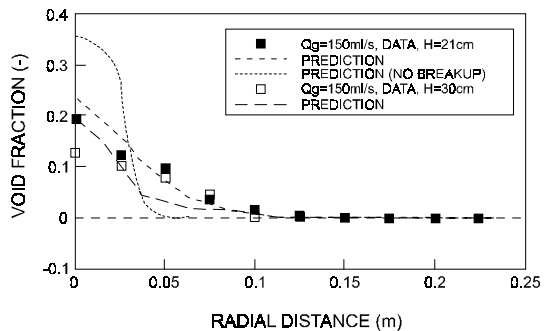


Figure 4: Comparison of the void fraction as a function of distance from the plume centre between models and experimental data.

Ladle Configurations

Guo and Irons extended this work into three dimensions, and fully accounted for the momentum jump conditions. The momentum equation for the bubble, written in vector notation, is:

$$(\rho_g + \rho_l C_{VM}) \cdot V_{\text{bubble}} \left(\frac{\partial \vec{V}_b}{\partial t} \right) = \vec{F}_B + \vec{F}_D + \vec{F}_L - V_{\text{bubble}} \nabla P + V_{\text{bubble}} \rho_l C_{VM} \vec{V}_l \cdot \nabla \vec{V}_l \quad (1)$$

where the term $\rho_l C_{VM}$ is the virtual (or added) mass of the bubbles. The body and interfacial forces in Equation (1), *viz.* the buoyancy force, the drag force, and the lift force, are defined as:

$$\vec{F}_B = (\rho_l - \rho_g) \cdot V_{\text{bubble}} \cdot \vec{g} \quad (2)$$

$$\vec{F}_D = -\frac{3}{4} \frac{C_D \rho_l}{d_{\text{bubble}}} V_{\text{bubble}} \vec{V}_R \left| \vec{V}_R \right| \quad (3)$$

$$\vec{F}_L = -C_L \rho_l V_{\text{bubble}} \vec{V}_R \times \nabla \times \vec{V}_l \quad (4)$$

where the relative velocity is the difference between gas and liquid instantaneous velocities:

$$\vec{V}_R = \vec{V}_g - \vec{V}_l \quad (5)$$

The last term in Equation (1) is due to the fact that the added mass is also under the action of forces exerted on the liquid phase, and the sum of which equals to the product of its mass and the liquid phase acceleration, given by $\vec{V}_l \cdot \nabla \vec{V}_l$.

In an Eulerian framework the Navier-Stokes Equation for the liquid can be written as:

$$\begin{aligned} \frac{d_l}{dt} (\alpha \rho \vec{V})_l - \nabla \cdot (\alpha \mu_{\text{eff}} \nabla V)_l \\ = -\alpha_l \nabla P + \vec{M}_L + \vec{S}_V \end{aligned} \quad (7)$$

The inter-phase transfer forces are contained in M_L :

$$\vec{M}_L = \vec{F}_D + \vec{F}_L + \vec{F}_{VM} \quad (8)$$

which are the drag, lift and virtual mass terms, respectively:

$$\vec{F}_D = \frac{3}{4} \frac{C_D \rho_l \alpha_g}{d_{\text{bubble}}} \vec{V}_R \left| \vec{V}_R \right| \quad (9)$$

$$\vec{F}_L = C_L \alpha_g \rho_l \vec{V}_R \times \nabla \times \vec{V}_l \quad (10)$$

$$\vec{F}_{VM} = \alpha_g C_{VM} \rho_l \left(\frac{d_g}{dt} \vec{V}_g - \frac{d_l}{dt} \vec{V}_l \right) \quad (11)$$

It can be shown that Equations (9) to (11) are consistent with Equations (3) and (4), and the relevant terms in

Equation (1), in terms of conservation of momentum across the bubble interfaces.

The governing equation for other liquid phase variables, such as velocity, turbulent kinetic energy and the turbulent kinetic energy dissipation rate, in its general form, is:

$$\frac{\partial}{\partial t} (\alpha \rho \Phi)_l + \nabla \cdot (\alpha \rho \vec{U} \Phi)_l = \nabla \cdot \left(\alpha \frac{\mu_{\text{eff}}}{\sigma_\Phi} \nabla \Phi \right)_l + S_\Phi \quad (13)$$

which take on their conventional forms for Eulerian formulations. The SIMPLE scheme, developed by Patankar, was used for the liquid phase. The instantaneous velocity of the liquid is the sum of the time-averaged velocity and the fluctuating component; the latter is calculated as:

$$\vec{U}_f = \xi \sqrt{\frac{2}{3} k} \quad (14)$$

where ξ is a random number with a Gaussian distribution, as developed by Johansen and Boysan. This time-varying velocity is used in the bubble equations to generate the bubble trajectories in a stochastic manner.

Two cases were used for the model validation: gas injection into a Woods metal bath as performed by Xie and Oeters, and a water model in our laboratory. For the Woods metal the calculation domain covered half of the ladle, taking advantage of the mirror symmetry. The grid numbers were 32×20×15 in angular×radial×vertical directions. The number of tracked bubbles was 1000 for nozzle injectors, and 10000 for porous plugs. Convergence was considered to be achieved when the accumulated residuals for all variables fell below 4×10^{-3} .

The calculated gas void fraction at plume centre is given in Figure 5, together with measured data. A reasonable agreement between the two is observed. Calculated void fractions are somewhat lower than measured values, especially near the bottom. This may be due to the fact that the bubble break up criterion used in the model is based on water model study, and that may not be the best description for the situation in Woods Metal.

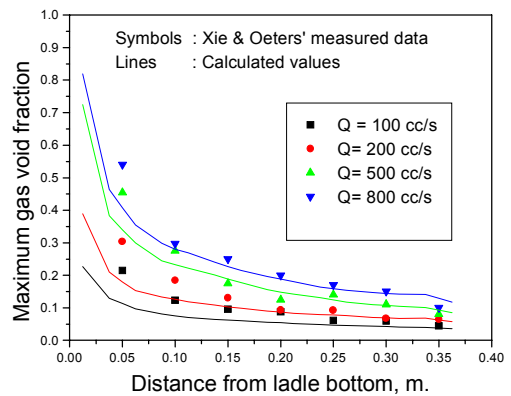


Figure 5: Comparison between calculated and measured maximum gas void fraction.

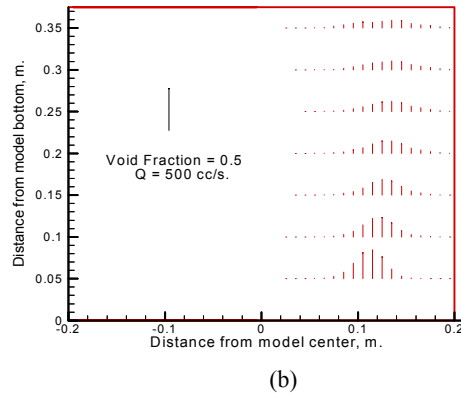
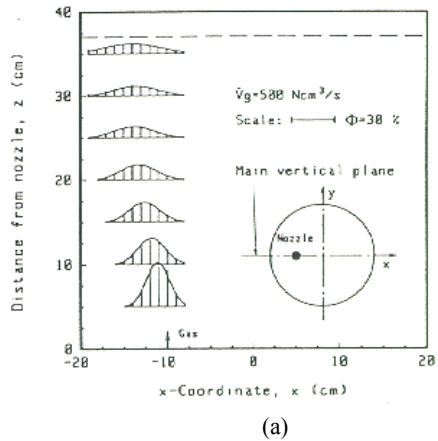


Figure 6 Comparison of measured and calculated plume position and void fraction
 (a) measured by Xie & Oeters (b) calculated

Figure 6 gives the calculated plume position and void fraction distribution at the symmetrical plane, for the case of gas injection rate of 500 cm³/s., together with Xie and Oeters' data. Agreement between the two is satisfactory.

By examining the magnitude and direction of the various terms in Equation (1), it is apparent that the lift force is responsible for the radial bubble spreading from the plume centre, while the lateral drag force mainly influences plume bending. Once the liquid lateral velocity becomes comparable to the rising speed of the bubbles, lateral displacement of bubbles caused by drag becomes sensible, and plume bending is observed.

The calculated dependency of plume displacement on gas flow rate is higher than that observed by Xie and Oeters. At lower flow rates the plume centre displacement tends to be smaller than measured. This is because the calculated horizontal velocity components are smaller for these cases, causing less plume displacement. This disagreement should be further examined.

Figure 7 gives the comparison between calculated and measured maximum vertical liquid velocities at the plume centre for Xie and Oeters' experiment. They are in good agreement, except near the bath surface, where the calculated value is lower. This is because the assumed flat free surface forces liquid to turn earlier than it does in reality.

Figure 8 gives the velocity direction and magnitude at the bath surface, the symmetrical plane, and near the ladle wall, showing that gas lifted liquid rises along the ladle wall, instead of a strictly vertical cone. It then turns towards at the opposite wall. There is a stagnant zone near the top surface, right opposite to the injector's position.

Comparing these figures with measured the results obtained by Xie and Oeters, it is clear that numerical simulations give very satisfactory results on liquid velocity, and fairly satisfactory results on plume displacement and gas void fraction. Therefore, the validity of predictions on fluid flow and gas void fraction of the model is established.

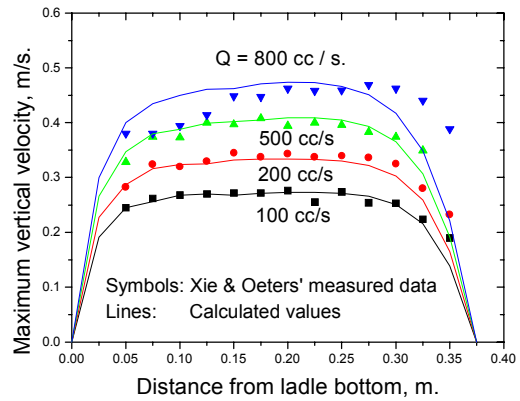


Figure 7 Comparison between calculated and measured maximum liquid velocity.

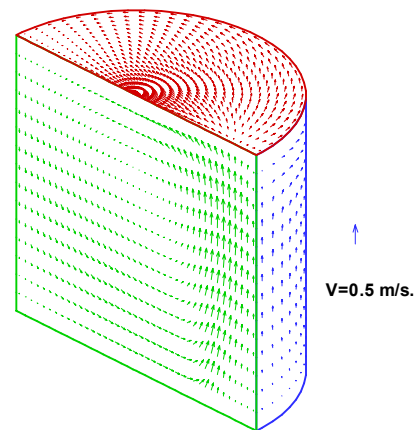


Figure 8 Calculated liquid velocity
 Woods Metal. Q=500 cc/s. r=0.5R.

For the model porous plug type injectors positioned at an angle of 75° and 45° to the symmetrical plane, and at a distance of 0.55R from the ladle centre were simulated. Figure 9 shows a photograph of observed plume bending

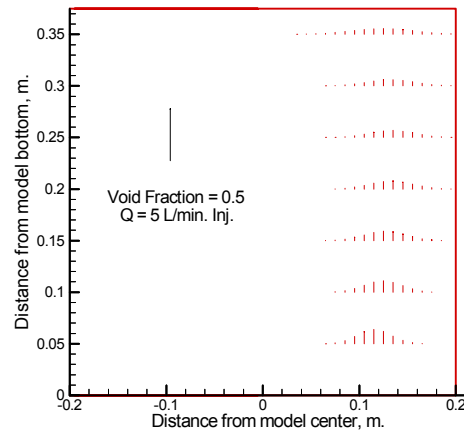
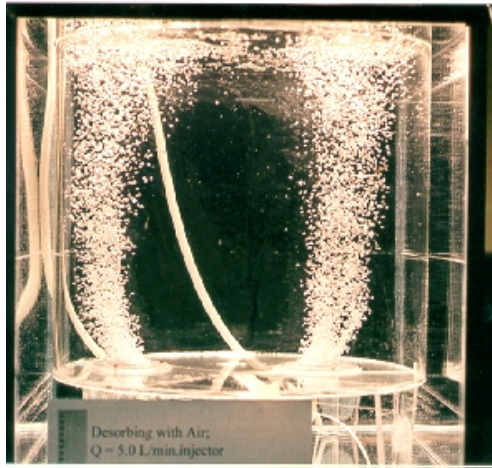


Figure 9 Observed and calculated plume position for water model.
 $Q=5\text{L/min. Plug, } \alpha=75^\circ$

in comparison with the calculated plume position and void fraction along the plume centre, associated with injectors at 75° . They are in reasonable agreement.

Electric Arc Furnace Configuration

These computational models have also been extended to electric arc furnaces (EAF) by Gu and Irons (1999). EAFs have captured a significant share of steel production due to lower production costs than the traditional integrated route, and due to advances in production technology, such as ultra-high power operation, oxygen injection and foamy slag practices, to name a few. Most of these improvements have occurred through in-plant development work, and it is clear that the operation of these furnaces has not reached its final optimum configuration. There have been few fundamental studies of heat transfer and fluid flow in EAFs. To reach the optimum operation requires a fundamental understanding of the phenomena occurring inside an electric furnace; the long-term goal of this research is to develop a comprehensive understanding of the internal workings of the furnace. This is a formidable task due to such complexities as the high-power electrical arc, foamy slag practices, unmelted or partially melted scrap of arbitrary shape, oxygen injection, and bottom stirring. The present work is the first step along the path; the effects of bottom stirring and carbon monoxide evolution are investigated, both experimentally and with mathematical modeling.

In this work a 1/3-scale Athin-slice@ model of Dofasco=190 tonne EAF was designed and constructed. The model allows fluid flow to be simulated in the bath for the arc jets, oxygen lancing, bottom stirring and CO evolution. The physical model is important because the physics of some flow phenomena particular to EAFs need to be visualized, understood and modeled properly. It was decided to build the model as a Athin-slice@ model because it would have been very difficult to simulate the foaming by a chemical reaction in a geometrically and chemically similar room temperature model. The model has a thickness of only 25 mm to allow for the introduction of gas through the back side, so that the gas can rise as small bubbles through the liquid in the model.

The model has controls to supply gas to a number of plenums, each having many 1 mm diameter holes as shown in Figure 10. The model can also simulate gas injection from bottom for soft stirring, oxygen lancing and arc jets, although only the results of foaming gas evolution and bottom stirring are presented in this paper.

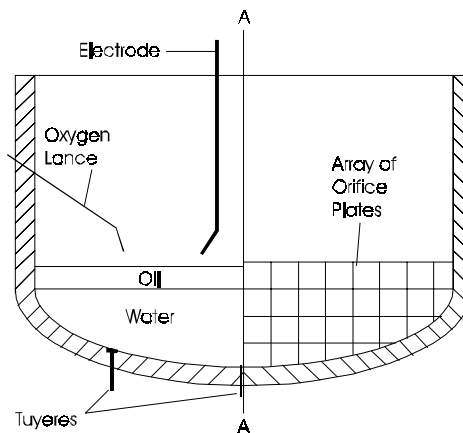


Figure 10 Schematic drawing of 2-D model. It should be noted that the model is symmetrical about the centerline AA. For clarity, the left side shows the injection equipment and the right side shows the orifice plates on the back side.

The liquid velocity was measured with Particle Image Velocimetry (PIV). Using this technique, the motion of tracer particles is captured with a digital camera. The particle velocity is assumed to be the liquid velocity. The two-dimensional nature of the thin-slice model is well-suited to this technique because only velocities perpendicular to the camera can be measured. The PIV system (see Figure 11) consists of a digital camera, including a frame grabber and commercial software. Polystyrene beads of effective diameter 0.5-1.0 mm (1.04 specific gravity) were used as tracer particles. The Stokes settling velocity of these particle is an estimate of the systematic error and the minimum velocity that can be detected (0.02 m/s for 1 mm diameter).

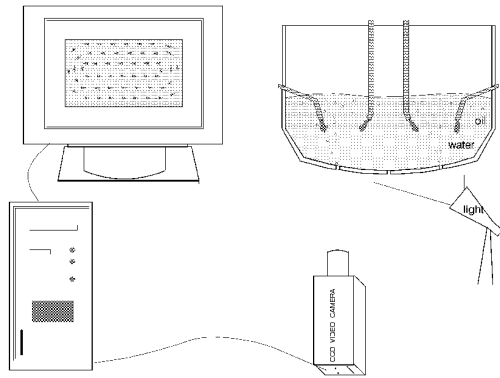


Figure 11 Schematic representation of the PIV system used in EAF water model

Once again Eulerian and Lagrangian two-phase models were compared against the physical model results. In this case, commercial software was used: Fluent (version 4.48) was selected for its Lagrangian sub-model, whereas Phoenix (version 2.2.2) was used for its Eulerian framework. The governing equations were similar to those already presented.

Figure 12a shows the PIV-measured mean liquid velocity field for soft bottom stirring. Two injectors were operated in a symmetrical manner, so only half of the model is shown. It was not possible to make measurements inside the plume, so it is represented as the dark region. Circulation loops on either side of the plume can be seen. The plume was distorted in shape due to its confinement in this thin slice model; free, unconfined plumes rise vertically with radial symmetry. Due to the waves formed at the bath surface, the flow was rather turbulent in this region. Very small bubbles were also found in the regions close to the bath surface.

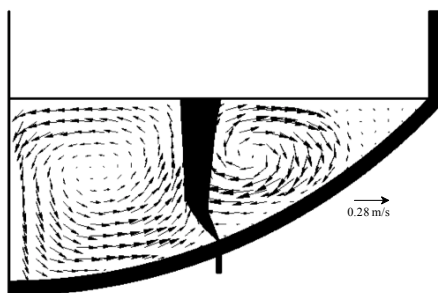


Figure 12a Measured mean velocity distribution with gas injection from two bottom tuyeres at the flow rate of 6.0 slpm

The corresponding numerical simulations with the Lagrangian and Eulerian models are shown in Figures 12b and 12c, respectively. The general features of the flow such as the bending of the plume and the two circulation loops are well-represented. The loop on the right hand side is stronger with the Lagrangian model than with the Eulerian one. To make a more quantitative comparison, velocities along two lines are compared: a vertical line bisecting the vertical symmetry plane, (Figure 13a), and a vertical line in the centre of the model 300 mm from this plane (Figure 13b). In both cases, the Eulerian model

overestimates the velocities, and the Lagrangian model reproduces the experimental results quite well.

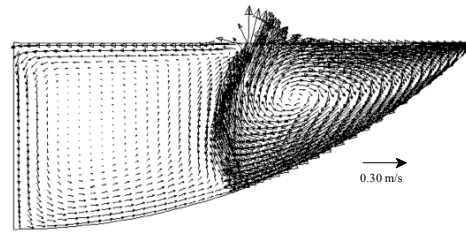


Figure 12b Computed velocity distribution (in the centre of the model) with Lagrangian model with gas injection from two bottom tuyeres (6.0 slpm)

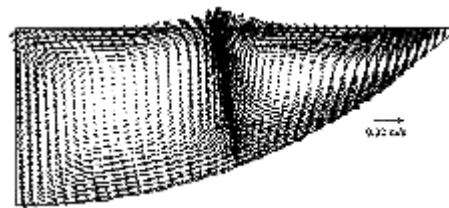


Figure 12c Computed velocity distribution (in the centre of the model) with Eulerian model with gas injection from two bottom tuyeres (6.0 slpm)

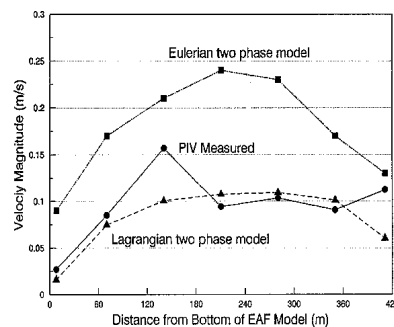


Figure 13a Measured and computed velocity (absolute magnitude) in the Centre plane of the model with gas injection from two bottom tuyeres at the flow rate of 6.0 slpm.

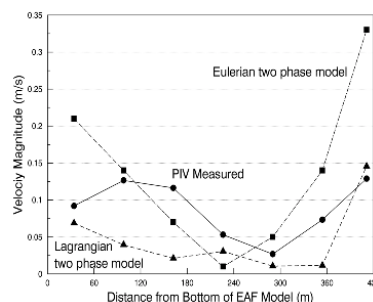


Figure 13b Measured and computed velocity (absolute magnitude) 300mm from the Centre plane of the model with gas injection from two bottom tuyeres at the flow rate of 6.0 slpm.

The present physical model provides a demanding test of the mathematical models. The plume bending is an artefact of the confinement of the plume that is not observed in unconfined configurations. Nevertheless, both models exhibited some bending in their results; however, the Lagrangian model gave results that were closer to the experimental results in plume shape and liquid velocity. It is also apparent that the Lagrangian model gave a better representation of the plume. In the Eulerian model, there was more spreading of the plume from bottom injection than in the model, and there were problems with numerical diffusion of the gas that is a fundamental problem with the Eulerian framework. Furthermore, the Eulerian model was not capable of properly handling the introduction of the gas through the back surface of the physical model; instead of discrete bubbles, the gas was modeled as a low velocity continuous film of gas.

In terms of future requirements the Lagrangian approach is also superior. It can easily accommodate changes in bubble size that may occur due to coalescence, heat transfer or mass transfer. The Lagrangian model is also amenable to the treatment of free surface phenomena by techniques such as the volume-of-fluid method. This will be important for the simulation of slag-metal interfaces and the treatment of jets from oxygen lances or the electrical arcs. It was also found that the Lagrangian approach is more economical in computational programming effort, computer memory requirements and processing time.

SLAG FOAMING

Introduction

Slag foaming is a term that is used loosely in the metallurgical industry to describe the expansion of the slag phase due to gas, usually generated by a chemical reaction. Most commonly the reaction is between oxygen and carbon to form carbon monoxide. The oxygen may be injected through a lance or may be in the form of iron oxide dissolved in the slag. The carbon may be in the form of injected carbon, char suspended in the slag or carbon dissolved in iron droplets in the slag. At very low rates of gas evolution, the slag foams resemble beer or soap foams, having void fractions of 0.9 or greater. In these situations, the physico-chemical properties of the slag have a large influence on the stability of the foam. These conditions are seen in the upper left portion of Figure 14 (Gou *et al.*). As the gas flow rate is increased, turbulence destroys the delicate foam cell walls. For liquids that are not naturally foamy, *i.e.*, pure liquids, the void fraction increases with gas flow rate, also shown in Figure 14, so that at high velocity, the void fraction approaches unity. The data shown in this Figure was taken from smelting/reduction vessels. Huge gas flow rates are generated from the smelting reactions that lift the slag in a manner more akin to a fluidized bed than a soap foam; the superficial gas velocity is of the order of 1 m/s. Electric furnaces operate with lower superficial velocities, approximately 0.1 m/s, in a regime where conventional foams may exist.

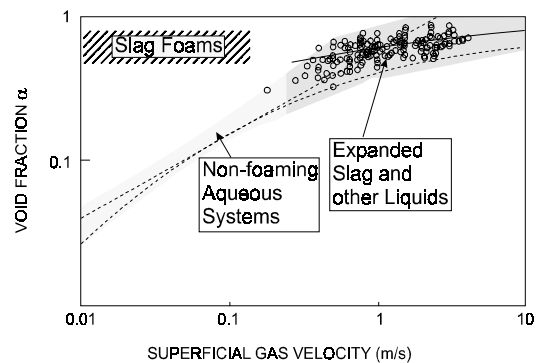


Figure 14: Summary of superficial gas velocity-void fraction relationships for foaming and non-foaming systems, from Gou *et al.*

Physical and Mathematical Modelling of Foaming

At our present level of understanding of foaming, it is not possible to calculate *a priori* exactly where it occurs. Therefore, it was decided to inject the gas through the holes in the back of the model at two symmetrical locations in the model. One of these locations is shown in Figure 15a. While this location is close to the point where an oxygen lance would impinge on the melt, it is not necessarily a quantitative representation of an actual furnace; the present experiments are carried out to investigate the general flow phenomena, and assure that they are captured with the mathematical model. On-going work with modeling the oxygen jet trajectory will permit *a priori* specification of the location of decarburization.

Figure 15a shows the foaming region in the bath with a gas injection rate of 164 slpm. There is very strong upwelling into this two-phase region, and strong recirculation. The corresponding measured velocity distribution is shown in Figure 15b. It was not possible to make PIV measurements in the two-phase region, so this is represented by the grey regions. Note that the foaming region rises several centimeters above the quiescent level due to the gas lift. The measured velocities show that the gas creates a very strong circulation loop with velocities of the order of 0.15m/s immediately beneath the foam.



Figure 15a Gas foaming with two CO evolution zones at the flow rate of 164 slpm

The gas in the Lagrangian model rises in the centre of the model, whereas the gas rises close the injection wall in the Eulerian model. The numerically simulated results are displayed in Figure 15c (in the centre of the model) from the Lagrangian model and Figure 15d (close to the injection wall) from the Eulerian model. Both models reproduce the large circulation loop close to the centre of the model. However, it seems that the fluid flow just below the bubbly foaming region is better computed by the Eulerian model (see Figure 15d) than by the Lagrangian model (see Figure 15c) where a small circulation loop is formed.

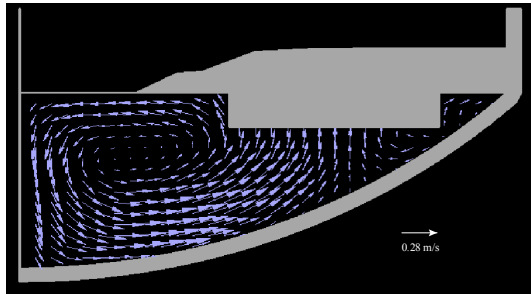


Figure 15b Measured mean velocity distribution with two CO evolution zones at the flow rate of 164 slpm.

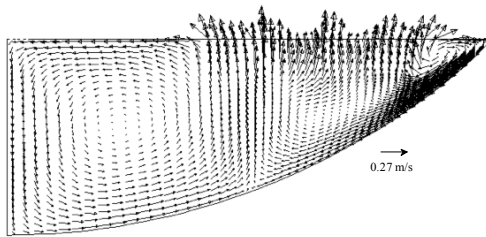


Figure 15c Computed velocity distribution in the centre of the model with the Lagrangian model with two CO evolution zones (164 slpm)

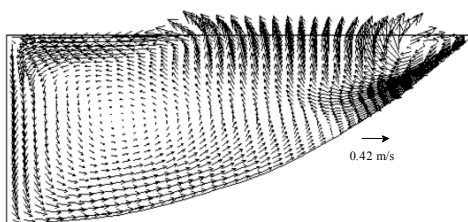


Figure 15d Computed velocity distribution close to injection wall with the Eulerian model with two CO evolution zones (164 slpm)

A more quantitative comparison is made at the same two locations as for Figures 13a and b in Figures 16a and b. At the centre of the model, Figure 16a shows that the Lagrangian model gives excellent agreement with the experimental results, whereas the agreement is not as good at the 300 mm (Figure 16b). The Eulerian model generally over-predicts the liquid velocities.

Injection of gas through a large number of 1 mm diameter holes in the back side can be well simulated using the Lagrangian model as seen in Figure 17 where the velocity

distribution, bubble trajectories and concentration in the cross section of the model are displayed. 180 bubbles (corresponding to 180 injection points) were injected into the model and the bubbles rose upwards close to the center of the model. This produced the higher bubble concentration in the center of the model. Although there is some back-mixing in the bubbly region (see Figure 17a), the fluid flow below the bubbly region is relatively uniform due to its Athin-slice@ nature.

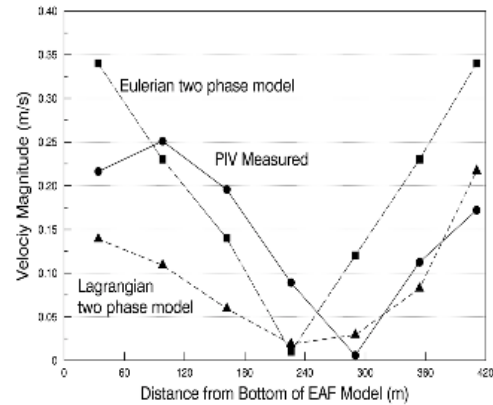


Figure 16a Measured and computed velocity (absolute magnitude) in the *Centre* plane of the model with two CO evolution zones at the flow rate of 14 slpm

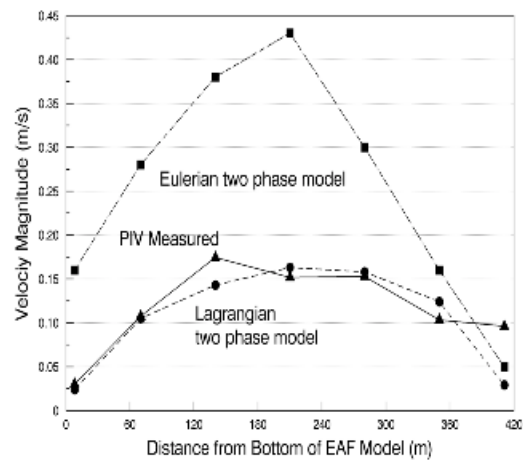


Figure 16b Measured and computed velocity (absolute magnitude) 300 mm from the *Centre* plane of the model with two CO evolution zones at the flow rate of 164 slpm

In the Eulerian framework, it was impossible to simulate individual bubbles as in the Lagrangian model. The prescribed gas flow was evenly distributed across the injection wall, so that the gas phase velocity was much lower than the actual velocity through the 1 mm holes in the physical model. This is equivalent to Apouring@ the gas into the model. Consequently, the gas rose more like a film close to the injection wall. Figure 18b shows that the highest gas volume fraction is 0.72 near the injection wall. This computation is at odds with the experimental observation of discrete bubbles. Because the gas is so concentrated on the injection wall, there is much more

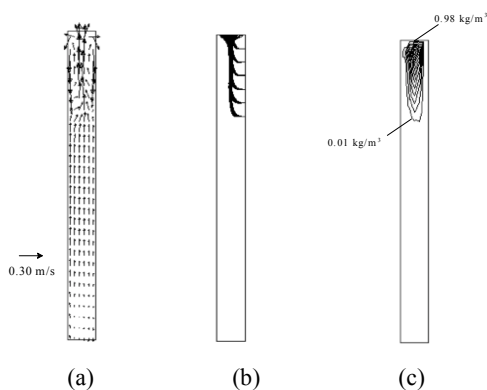


Figure 17 Computed velocity distribution (a); random bubble trajectories (b) and the bubble concentration (c) with the Lagrangian model in the middle cross section of the model with two CO evolution zones (164 slpm).

downflow over the front wall than with the Lagrangian model that does not represent the real situation. This is a severe limitation of the Eulerian model.

The present work gives considerable insight into the physical aspects of foaming gas behavior. The bubbles in the present model were quite small, and it is also expected that the carbon monoxide bubbles generated *in situ* are also very small. These small bubbles couple very well with the liquid to provide very strong, gas-lift pumping action. It must also be pointed out that the real situation is more complex because of the presence of both slag and metal, and most of the gas is generated in the slag. Work is underway to incorporate these aspects with the volume-of-fluid free surface method.

It is well-accepted that bottom-stirring is essential for BOF steelmaking, but it has not been widely adopted in EAF steelmaking even though many of the same fundamental advantage apply, mainly related to closer chemical and thermal equilibrium between slag and metal. The configuration in an EAF is considerably different; the bath is shallower and it is harder to maintain the injection points due to the scrap charges. The characteristics of the bottom stirring will change as the scrap melts, and there will be important interactions among the four principle sources of stirring: the bottom, the foamy slag, the oxygen lances and the arcs. It is anticipated that the future work in this area will shed some light on these issues.

CONCLUSIONS

Three-dimensional numerical simulations of foaming gas evolution and bottom stirring were performed using Lagrangian and Eulerian models, and comparisons were made with the measured results. Generally, the Lagrangian model gave a better representation of the fluid flow for both bottom stirring and foaming gas evolution. The models are capable of properly representing complex phenomena, such as plume spreading and bending. The Lagrangian model has distinct advantages over the Eulerian method in terms of simplicity of formulation, ability to accommodate changes in bubble size due to

coalescence, heat transfer or mass transfer, computer memory requirements, and computational effort. Furthermore, the Lagrangian model is more easily extended to handle free-surface effects that are important for the arc jetting and oxygen lancing modeling to be tackled in the near future. Finally, the article highlights the need for careful evaluation of CFD models.

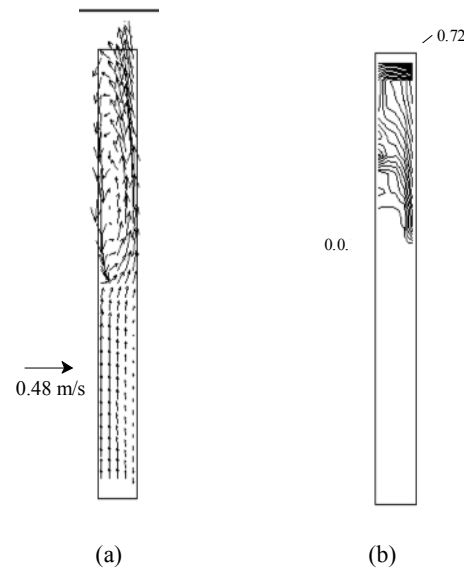


Figure 18 Computed velocity distribution (a), and bubble volume fraction (b) with the Eulerian model in the middle cross section of the model with two CO evolution zones (164 slpm)

REFERENCES

- GOU, H., IRONS, G.A. and W.-K. LU, AA multiphase fluid mechanics approach to gas holdup in bath smelting processes@, *Metall. Trans. B*, 1995, Vol.26B, p.1.
- Gu, L. and Irons, G.A., unpublished research, 1999.
- GUO, D.C. and IRONS, G.A. unpublished work, 1999.
- JOHANSEN, S. T. and BOYSAN, F., "Fluid dynamics in bubble stirred ladles: Part II. Mathematical modeling", *Metal. Trans.*, Vol. 19B, Oct. 1988, p.755.
- MAZUMDAR, D. and R. I. L. GUTHRIE, "An assessment of a two phase calculation procedure for hydrodynamic modeling of submerged gas injection in ladle", *ISIJ International*, Vol. 34(1994), No.5 P. 384.
- SHENG and IRONS, G.A., AThe impact of bubble dynamics on the flow in plumes of ladle water models@, *Metall. Trans. B*, 1995, Vol.26B, p.625.
- SHENG, Y. and IRONS, G. A., "The impact of bubble dynamics on flow in plumes of ladle water models", *Metal. Trans.* Vol. 26B, June 1995, p. 625.
- SHENG, Y.Y. and IRONS, G.A., AMeasurement of the internal structure of gas-liquid plumes@, *Metall. Trans. B*, 1992, Vol.23B, p.779.
- SHENG, Y.Y. and IRONS, G.A., AMeasurement and modeling of turbulence in the gas/liquid two-phase zone during gas injection@, *Metall. Trans. B*, 1993, Vol.24B, p.695
- XIE, Y. and OETERS, F., "Measurement of bubble plume behaviour and flow velocity in gas stirred liquid woods metal with an eccentric nozzle position", *Steel Research*, Vol. 65, No. 8, 1994, P. 315.

